Multiple universalities in order-disorder magnetic phase transitions

H. D. Scammell and O. P. Sushkov

School of Physics, The University of New South Wales, Sydney, NSW 2052, Australia

Phase transitions in isotropic quantum antiferromagnets are associated with the condensation of bosonic triplet excitations. In three-dimensional quantum antiferromagnets, such as TlCuCl₃, condensation can be either pressure or magnetic field induced. The corresponding magnetic order obeys universal scaling with thermal critical exponent ϕ. Employing a relativistic quantum field theory, the present work predicts the emergence of multiple (three) universalities under combined pressure and field tuning. Changes of universality are signaled by changes of the critical exponent ϕ. Explicitly, we predict the existence of two new exponents $\phi = 1$ and $1/2$ as well as recovering the known exponent $\phi = 3/2$. We also predict logarithmic corrections to the power law scaling.

I. INTRODUCTION

Pressure and magnetic field induced condensate phases in quantum magnetic systems have become instrumental to our understanding of universal, critical phenomena. A great effort (experimental, numerical, and theoretical) has been devoted to uncovering and categorizing the universal features of critical magnetic condensate phases. The present work considers three-dimensional (3D) quantum antiferromagnets (QAFs), where the combined interplay between pressure, magnetic field, and temperature (p,B,T) remains theoretically unexplored, yet offers an exiting arena for theorists and experimentalists alike to uncover new universal behavior. In Fig. 1 we present the generic phase diagrams of dimerized QAFs such as TlCuCl₃, KCuCl₃, and CsFeCl₃. Figure 1(a) shows the magnon Bose condensation (BEC) line in the field-pressure diagram, and Fig. 1(b) shows the antiferromagnetic (AFM) transition line in the temperature-pressure diagram. It is also instructive to look at Fig. 2 which shows the 3D (p,B,T) phase diagram. The point of primary interest is the critical field-critical temperature power law,

$$\text{a: } \delta B_{\text{BEC}} \sim T^{\phi}, \quad \text{b: } \delta T_N \sim B^{1/\phi}. \quad (1)$$

The shift of the BEC transition line at small temperature is shown schematically in Fig. 1(a); while the shift of the AFM/Néel transition line at small field is in Fig. 1(b).

It is widely believed that at $p < p_c$, $\phi = 3/2$ is the universal BEC exponent, which can be obtained from the scaling arguments on the dilute Bose gas [1,2] or explicitly for magnon BEC [3,4]. For a review see [5]. On the other hand, experiment (on TlCuCl₃ and KCuCl₃ [6–9]) and numerics [10] show $1.5 \leqslant \phi \lesssim 2.3$, depending crucially on which temperature range is used for fitting [5,11]. We understand recent data on 3D QAF CsFeCl₃ [12], taken along the thick blue-red solid lines in Fig. 2, as a hint for a significant and unexpected evolution of the index ϕ along the line.

The primary goal of the present work is to derive the evolution of the critical index ϕ across the phase diagram. Another goal is to explain why the index depends on the fitting range; even if *a priori* the range seems to be very narrow. We will show that answers to both questions are related to the quantum critical point $(p,B,T) = (p_c,0,0)$. Ultimately, the quantum

critical point (QCP) governs the evolution of the critical index ϕ across the phase diagram. This is illustrated in Fig. 2.

Previous theoretical approaches were concentrated at the BEC transition, $p < p_c$. They employed a dilute Bose gas model [4,5] and/or bond-operator technique [13]. In the end, these techniques rely on the Hartree-Fock-Popov approximation, yet it is known that the Hartree-Fock-Popov approximation breaks down in the vicinity of a critical point [14]. In the present work we employ a quantum field theory approach which naturally describes quantum critical points.

II. METHODS

The quantum phase transition (QPT) between ordered and disordered phases is described by the effective field theory with the following Lagrangian [15,16]:

$$\mathcal{L} = \frac{1}{2}(\partial_t \vec{\varphi} - \vec{\varphi} \times \vec{B})^2 - \frac{1}{2}(\vec{\nabla}\vec{\varphi})^2 - \frac{1}{2}m_0^2\vec{\varphi}^{\,2} - \frac{1}{4}\alpha_0\vec{\varphi}^{\,4}. \quad (2)$$

The vector field $\vec{\varphi}$ describes staggered magnetization, B is an external applied field, and for now we set $g\mu_B = 1$. We now briefly outline the *mean-field* phase transitions captured by this Lagrangian. Consider first $B = 0$, the pressure induced QPT results from tuning the mass term m_0^2 for which we take the linear expansion $m_0^2(p) = \gamma^2(p_c - p)$, where $\gamma^2 > 0$ is a coefficient and p is the applied pressure. Varying the pressure leads to two distinct phases. (i) For $p < p_c$ we have $m_0^2 > 0$, and the classical expectation value of the field is zero $\varphi_c^2 = 0$. This describes the magnetically disordered phase, the system has a global $O(3)$ rotational symmetry, and the excitations are gapped and triply degenerate. (ii) For pressures $p > p_c$ we have $m_0^2 < 0$, and the field obtains a nonzero classical expectation value $\varphi_c^2 = \frac{|m_0^2|}{\alpha_0}$. This describes the magnetically ordered, antiferromagnetic phase. Varying m_0^2 from positive to negative spontaneously breaks the $O(3)$ symmetry of the system.

Next consider nonzero B at fixed $p < p_c$: For $B < B_c = m_0$ the system has $O(2)$ symmetry, and the degeneracy of the triplet modes is lifted by Zeeman splitting. The field induced QPT results from tuning $B^2 > m_0^2 = \gamma^2(p_c - p)$, this corresponds to the blue line in the (B,p) plane, Fig. 2. The condensate field is given by $\varphi_c^2 = \frac{B^2 - m_0^2}{\alpha_0}$ and always lies in the
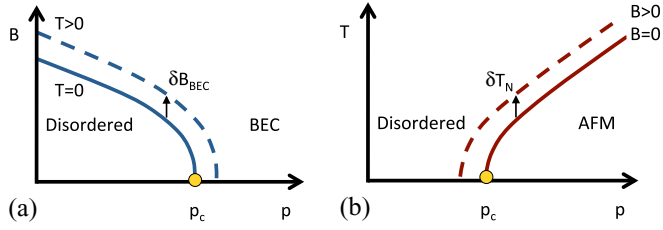
FIG. 1. Critical field and temperature power law shifts. (a) Shift of critical field-pressure line with temperature $\delta B_{BEC} \sim T^\phi$. Solid blue curve is at zero temperature, dashed blue at nonzero temperature. (b) Shift of critical (Néel) temperature-pressure line with field $\delta T_N \sim B^{1/\phi}$. Solid red curve is at zero field, dashed red at nonzero field.

plane perpendicular to $\vec{B}$. At $B = 0$, $p > p_c$ and $T < T_N$, the AFM condensate (staggered magnetization) has an arbitrary orientation. Application of a magnetic field, even vanishingly small, acts to globally reorient the system such that the AFM condensate is perpendicular to the applied field $\vec{\varphi}_c \perp \vec{B}$. Without loss of generality, one may assume that the condensate for $p > p_c$, $T < T_N$ has a given orientation $\vec{\varphi}_c$, and that the magnetic field is applied perpendicular to this predefined direction. Of course, mathematically, this does not alter any conclusions of the paper. To determine the order-disorder (BEC or AFM) transition line one can approach the transition starting from either the ordered or disordered phase. In this work we start from the latter; all results are derived starting from disordered phase. There are three magnetic excitations with ladder polarization $\sigma = -,0,+$. The polarization is the projection of angular momentum on the direction of magnetic field. In Fig. 3 we summarize the results for the evolution of the three mode gaps through the field and pressure quantum phase transitions, separately. Explicit parameters correspond to those found in Ref. [19] for TlCuCl$_3$. Here we disregard the small easy-plane anisotropy seen in TlCuCl$_3$, which has been shown to have negligible influence on the critical properties [19], see also comment [20].
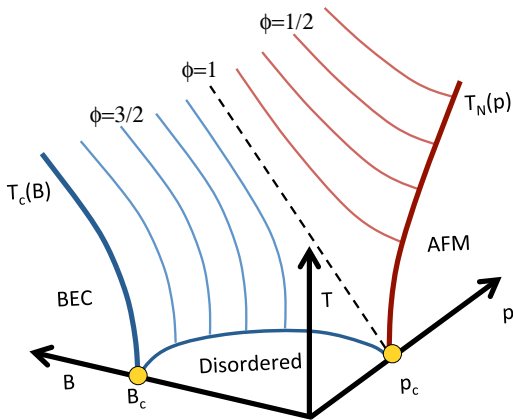

FIG. 2. Multiple universalities in the (p,B,T) phase diagram. Blue curves correspond to the BEC transition lines; here $p < p_c$ and the critical exponent is $\phi = 3/2$. Red curves correspond to the Néel transition lines; here $p > p_c$ and the critical exponent is $\phi = 1/2$. The dashed, black curve shows the critical pressure transition line, with critical exponent $\phi = 1$.
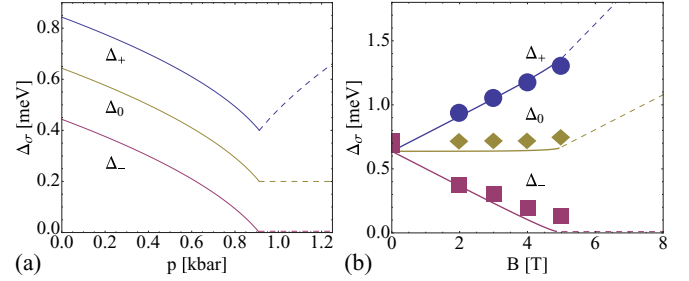

FIG. 3. Excitation gaps Δ_σ: (Left) pressure driven at fixed field $B = 0.2$ meV and $T = 0$. (Right) field driven at $p = 0$ kbar and $T = 1.5$ K. Solid lines are theoretical results derived in this paper. Markers indicate experimental data for TlCuCl$_3$ [17,18].

Beyond mean field: Everywhere in the text $m_0^2 = \gamma_0^2(p_c - p)$ and α_0 represent the zero temperature mass tuning parameter and coupling constant without quantum fluctuation corrections. Taking into account quantum and thermal fluctuation corrections due to interaction term $\frac{1}{4}\alpha_0\vec{\varphi}^4$, we will denote the renormalized parameters $m_0^2 \to m_{\Lambda,\sigma}^2$ and $\alpha_0 \to \alpha_\Lambda$. The explicit form for $m_{\Lambda,\sigma}^2 = m_{\Lambda,\sigma}^2(p,T,B)$ depends on the location within the phase diagram, and polarization σ. Full details are presented in Appendixes B and C, while expressions are presented below. The strength of the coupling α_Λ determines the strength of all interactions in the theory, and is dependent on the energy scale Λ. Generically, the one-loop renormalized coupling takes the form [19,21]

$$\alpha_\Lambda = \frac{\alpha_0}{1 + 11\alpha_0/(8\pi^2)\ln(\Lambda_0/\Lambda)}. \quad (3)$$

Specifically for the problem at hand, the coupling runs with scale $\Lambda = \max\{m_{\Lambda,\sigma}, B, T\}$. Accordingly, there is just a single point on the phase diagram at which all energy scales vanish $\Lambda \to 0$; the quantum critical point $(p_c,0,0)$, see Fig. 2. At this point the coupling runs to zero $\alpha_\Lambda \to 0$ (asymptotic freedom). The running of the coupling constant will play an essential role in resolving our main goals/questions: Why the index ϕ depends on the location within the phase diagram, and why the expected index $\phi = 3/2$ in the BEC regime depends on the fitting range?

In the disordered phase the Euler-Lagrange equation with (2) results in the following dispersion:

$$\omega_k^\sigma = \sqrt{k^2 + m_{\Lambda,\sigma}^2} + \sigma B, \quad (4)$$

where $m_{\Lambda,\sigma}$ is the renormalized mass. Note that the σB term is not renormalized. This is a consequence of a Ward identity (Larmor theorem). While the stationary states (4) have a fixed ladder polarization, technically it is more convenient to calculate fluctuation corrections in the Cartesian basis $\vec{\varphi} = (\varphi_x, \varphi_y, \varphi_z)$. Let us denote by $\mathcal{V}$ the part of the Lagrangian (2) independent of derivatives. Then, using a Wick decoupling of

the interaction term $\frac{1}{4}\alpha_0\vec{\varphi}^4$, in the single loop approximation we find

$$\frac{\partial^2 \mathcal{V}}{\partial \varphi_x^2} = m_0^2 - B^2 + 3\alpha_0\langle\varphi_x^2\rangle + \alpha_0\langle\varphi_y^2\rangle + \alpha_0\langle\varphi_z^2\rangle,$$

$$\frac{\partial^2 \mathcal{V}}{\partial \varphi_y^2} = m_0^2 - B^2 + \alpha_0\langle\varphi_x^2\rangle + 3\alpha_0\langle\varphi_y^2\rangle + \alpha_0\langle\varphi_z^2\rangle,$$

$$\frac{\partial^2 \mathcal{V}}{\partial \varphi_z^2} = m_0^2 + \alpha_0\langle\varphi_x^2\rangle + \alpha_0\langle\varphi_y^2\rangle + 3\alpha_0\langle\varphi_z^2\rangle, \quad (5)$$

where $\langle\varphi_x^2\rangle$ is the loop integral over the Green's function of field φ_x. An explicit calculation shows $\langle\varphi_x^2\rangle = \langle\varphi_y^2\rangle$, hence from Eqs. (A2), we have rather trivially satisfied the $O(2)$ Ward identity: $\partial^2 \mathcal{V}/\partial \varphi_x^2 - \partial^2 \mathcal{V}/\partial \varphi_y^2 = 0$. Further details are presented in Appendix A.

Quantum corrections corresponding to (A2) come from the scale $\Lambda < q < \Lambda_0$. Hence they must be accounted for via single loop renormalization group (RG). The thermal part of (A2) comes from $q \sim T$, hence here the simple single loop approximation is sufficient. All in all, calculations presented in Appendix C give

$$\frac{\partial^2 \mathcal{V}}{\partial \varphi_i^2} = m_{\Lambda,\pm}^2(T) - B^2, \quad \frac{\partial^2 \mathcal{V}}{\partial \varphi_z^2} = m_{\Lambda,0}^2(T), \quad (6)$$

where $\varphi_i = \{\varphi_x, \varphi_y\}$, and the renormalized masses are

$$m_{\Lambda,\pm}^2 = m_0^2\left[\frac{\alpha_\Lambda}{\alpha_0}\right]^{5/11} + \Sigma_T,$$

$$m_{\Lambda,0}^2 = m_0^2\left[\frac{\alpha_\Lambda}{\alpha_0}\right]^{5/11} + \alpha_\Lambda\sum_k 1/\omega_k^0\{n(\omega_k^+)$$

$$+ n(\omega_k^-) + 3n(\omega_k^0)\},$$

$$\Sigma_T \equiv \alpha_\Lambda\sum_k 1/\omega_k^0\{2n(\omega_k^+) + 2n(\omega_k^-) + n(\omega_k^0)\}. \quad (7)$$

Here $n(\omega_k) = 1/(e^{\frac{\omega_k}{T}} - 1)$, and we introduce the function Σ_T for brevity. Obviously expansions of Eqs. (7) in powers of B contain only even powers. Interestingly these expansions are different for $m_{\Lambda,\pm}$ and $m_{\Lambda,0}$. Therefore the relation $\omega_k^+ - \omega_k^0 = \omega_k^0 - \omega_k^-$, which is exact at $T = 0$, does not hold at nonzero T. At nonzero T the relation is valid only up to the linear in B approximation.

In a magnetic field, the condition of condensation follows from Eq. (4), $m_{\Lambda,\pm} - B_c = 0$. Using (7) this equation can be rewritten as

$$\Sigma_T = B_c^2 - m_0^2\left[\frac{\alpha_\Lambda}{\alpha_0}\right]^{5/11}. \quad (8)$$

III. RESULTS AND DISCUSSION

There are three distinct cases: (I) Above the critical pressure, when $T_c = T_N$, i.e., critical temperature equals the AFM/Néel temperature; (II) exactly at the critical pressure $p = p_c$; and (III) below the critical pressure, when $T_c = T_{BEC}$. At zero magnetic field, the critical temperature in case (I), Eq. (8), is identical to the equation for the Néel temperature derived in Ref. [19].
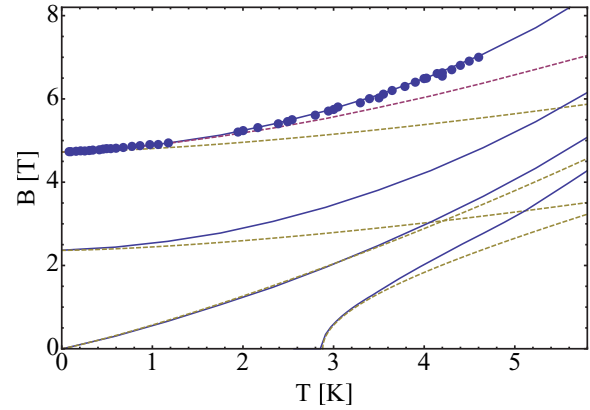

FIG. 4. Critical field vs temperature: Dashed yellow curves show solutions to scaling equations (9), (11), and (12). The dashed maroon curve shows a solution of (8) that accounts for thermal mixing of noncritical modes, but does not account for running coupling; coupling is at fixed value $\alpha_\Lambda \to \alpha_{\Delta_0} = 0.169 \times 8\pi$. Solid blue lines are the solution to (8) with a full account of noncritical modes and logarithmic running coupling. Blue points are experimental data from [9,22,23].

Consider case (I): $p > p_c$. In this case according to Eq. (1b) the Néel temperature varies in a weak magnetic field. To calculate Σ_T at $B \to 0$ we take the critical line dispersions $\omega_k^+ = \omega_k^- = \omega_k^0 = k$. Hence $\Sigma_T = \frac{5\alpha_\Lambda}{12}T^2$, where $T = T_{N0} + \delta T_N$; T_{N0} is the Néel temperature in zero magnetic field. Hence using Eq. (8) we find

$$(\text{I}):\delta T_N = \frac{6}{5\alpha_\Lambda}\frac{B^2}{T_{N0}} \quad \text{at } B \ll T_{N0}. \quad (9)$$

So the critical index in Eq. (1b) is $\phi = 1/2$.

In Ref. [19] the set of parameters describing TlCuCl$_3$ was determined:

$$p_c = 1.01 \text{ kbar}, \quad \gamma = 0.68 \text{ meV/kbar}^{1/2},$$

$$\frac{\alpha_0}{8\pi} = 0.23, \quad \Lambda_0 = 1 \text{ meV}. \quad (10)$$

When fitting experimental data in Ref. [19] the thermal line broadening had been accounted for via $\omega = k \to \omega = \sqrt{k^2 + \xi^2 T^2}$, $\xi = 0.15$. Therefore, if we use the set of parameters (10) to determine the value of the running coupling constant α_Λ, Eq. (3), the coefficient in (9) has to be corrected accordingly: $\frac{6}{5\alpha_\Lambda} \to 1.14\frac{6}{5\alpha_\Lambda}$. In Fig. 4 we illustrate Eq. (9) by a dashed yellow line originating from $T_{N0} = 2.8$ K. The coupling constant is $\alpha_\Lambda/8\pi = \alpha_{T_{N0}}/8\pi = 0.107$. For comparison, the solid blue line originating from 2.8 K represents the exact solution of Eq. (8) with a coupling constant running along the line.

Consider case (II), tuning exactly to the quantum critical point $p = p_c$, $T_{N0} = 0$. Again, to calculate Σ_T at $B \to 0$ we have to take the critical line dispersions $\omega_k^+ = \omega_k^- = \omega_k^0 = k$ and hence again $\Sigma_T = \frac{5\alpha_\Lambda}{12}T^2$. Substitution into (8) gives

$$(\text{II}): \quad B_c = \sqrt{\frac{5\alpha_\Lambda}{12}}T \quad \text{at} \quad B_c \ll T. \quad (11)$$

The condition $B_c \ll T$ is satisfied at sufficiently low temperatures since the coupling constants decays logarithmically, $\alpha_\Lambda \propto 1/\ln(\frac{\Lambda_0}{T})$. Hence in this case (II), the critical index of Eq. (1) is $\phi = 1$, and we find that, in addition to the exponent, there is nontrivial logarithmic scaling. In Fig. 4 we illustrate the asymptotic (11) by a dashed yellow line originating from $B = T = 0$. The solid blue line originating from the same point represents an exact solution of Eq. (8).

Finally we consider the BEC case (III), $p < p_c$. In this case only the ω_k^- dispersion branch is critical, $\omega_k^- \approx \frac{k^2}{2\Delta_0}$, where $\Delta_0 = B_0$ is the gap at $B = 0$. The other two branches are gapped. Calculation of Σ_T gives $\Sigma_T = \alpha_\Lambda \frac{\zeta(3/2)}{\pi\sqrt{2\pi}}\sqrt{\Delta_0}T^{3/2}$, where ζ is Riemann's ζ function. Hence, using Eq. (8) we find

$$\text{(III):} \quad \frac{\delta B_c}{\Delta_0} = \alpha_\Lambda \frac{\zeta(3/2)}{(2\pi)^{\frac{3}{2}}}\left(\frac{T}{\Delta_0}\right)^{3/2} \quad \text{at} \quad \delta B_c \ll \Delta_0. \quad (12)$$

As expected the critical index in Eq. (1a) is $\phi = 3/2$. To understand the region of validity of Eq. (12) we compare with TlCuCl₃ data [9,22,23]. The value of the gap at $T = p = B = 0$ is $\Delta_0 = m_{\Lambda,\pm} = 0.64$ meV [24]. The BEC critical field for $T = p = 0$ is $B_0 = 4.73$ T [25]. Hence, we obtain the g factor, which is defined as $B \rightarrow g\mu_B B$, $g = 2.35$ [20]. In Fig. 4 the dashed yellow line originating from $B_0 = 4.73$ T shows B_{BEC} versus T at $p = 0$ calculated with Eq. (12). The value of the coupling constant in this equation is obtained from Eqs. (3) and (10), $\alpha_\Lambda/(8\pi) = \alpha_{\Delta_0}/(8\pi) = 0.169$. Experimental data [9,22,23] are shown by circles. We see that Eq. (12) is valid only at $T \leqslant 1$ K.

There are two physical effects accounted for in (8), but neglected in (12). These are (i) the influence of the noncritical (gapped) modes ω_k^+, ω_k^0; and (ii) the logarithmic running of α_Λ. To illustrate the importance of noncritical modes, the dashed maroon line originating from 4.73 T in Fig. 4 shows a solution of Eq. (8) with an account of all three modes, but with a fixed coupling constant $\alpha_{\Delta_0}/(8\pi) = 0.169$. Finally, the solid blue line originating from 4.73 T shows a solution of (8) with an account of both (i) and (ii). Agreement with experiment is remarkable. We stress that there is no fitting in the theoretical curve. The set of parameters (10) was determined in Ref. [19] from data unrelated to magnetic field. To be consistent with this set when generating the solid blue and dashed maroon curves in Fig. 4 we use the same line broadening as in [19],

$$\omega_k^\sigma \rightarrow \sqrt{k^2 + m_{\Lambda,\sigma}^2 + \Gamma_T^2} + \sigma B, \Gamma_T = \xi T, \xi = 0.15.$$

Regimes (I) and (II) have never been considered before. On the other hand, the BEC regime (III) has been considered in a number of publications using the Hartree-Fock-Popov approximation for hard core bosons, from which simple $T^{3/2}$ dependence is predicted. Our conclusion is that such an approximation is only valid at vanishingly small temperatures and the region of validity shrinks to zero upon approaching the critical pressure QCP. This is illustrated in Fig. 4 by lines originating from points $B_0 = 4.73$ T and $B_0 = 2.36$ T at $T = 0$. Our exact theoretical solutions (blue solid lines) differ from the simple $T^{3/2}$ dependence (dashed yellow) due to two effects: influence the noncritical excitations and the running of the coupling constant. Both effects are governed by the magnetic quantum critical point $(p_c, 0, 0)$
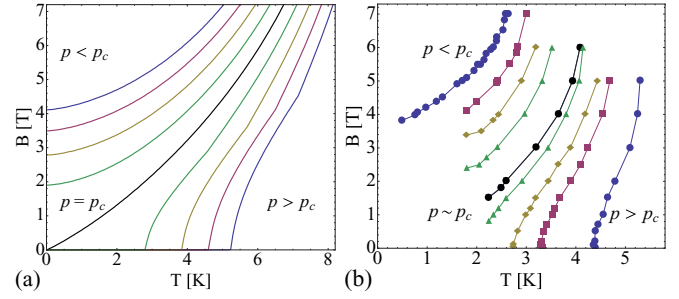

FIG. 5. Multiple universalities: Various curves show the critical field $B_c(T)$ at various pressures ranging from $p < p_c$, $p = p_c$, to $p > p_c$. (a) Solutions to (8) with parameters for TlCuCl₃. (b) Data for quantum antiferromagnet CsFeCl₃ [12].

and cannot be accounted for within a hard core boson model; whether it be Hartree-Fock-Popov approximation or even an exact solution. Including these effects, the present analysis resolves the long standing problem of the BEC critical exponent, which has been consistently reported at higher value $3/2 \leqslant \phi \leqslant 2.3$ [5–11].

The existence of three critical exponents $\phi = 3/2$, 1, and 1/2, and even logarithmic corrections to these exponents, is a readily testable result and constitutes our most important prediction for experiment. Figure 4 provides predictions directly for TlCuCl₃. In Fig. 5(a) we plot the predicted critical field in TlCuCl₃ vs temperature at various pressures. For comparison in Fig. 5(b) we present a similar experimental plot for quantum antiferromagnet CsFeCl₃ published very recently [12]. Unfortunately we cannot perform exact quantitative calculations (including all prefactors) for CsFeCl₃. Existing data for this compound are not sufficient to perform analysis similar to [19] for TlCuCl₃. However, the data [12] supports the proposed multiple critical exponent theory.

IV. CONCLUSION

In summary, employing a quantum field theoretic approach, our work predicts multiple critical exponents, and their corresponding logarithmic corrections, on the pressure, magnetic field, and temperature-phase diagram for 3D quantum antiferromagnets in the vicinity of the quantum critical point. For TlCuCl₃ we demonstrate remarkable agreement with existing data, and provide quantitative predictions for future experiments. We also resolve the long standing problem relating to the observed critical exponent in Bose-Einstein condensation of magnons.

APPENDIX A: GREEN'S FUNCTIONS AND PERTURBATIVE DECOUPLING

In the disordered phase we have the Lagrangian

$$\mathcal{L} = -\frac{1}{2}\begin{pmatrix}\varphi_1\\\varphi_2\\\varphi_3\end{pmatrix}^T\begin{pmatrix}\omega^2-k^2-(m^2-B^2) & -2i\omega B & 0\\ 2i\omega B & \omega^2-k^2-(m^2-B^2) & 0\\ 0 & 0 & \omega^2-k^2-m^2\end{pmatrix}\begin{pmatrix}\varphi_1\\\varphi_2\\\varphi_3\end{pmatrix} - \frac{\alpha}{4}\vec{\varphi}^4,$$

$$\mathcal{L} = -\frac{1}{2}\vec{\varphi}^T\hat{G}_D^{-1}\vec{\varphi} - \frac{\alpha}{4}\vec{\varphi}^4. \tag{A1}$$

We choose to work with real fields, in the Cartesian basis $\vec{\varphi} = (\varphi_x, \varphi_y, \varphi_z)$ and therefore do not diagonalize the kinetic matrix $\hat{G}^{-1}$. We are therefore left with anomalous Greens functions G_{xy}, G_{yx}, but they do not contribute to loop corrections to first order in α_0. The matrix $\hat{G}$ gives the bare Greens functions. We wish to calculate first order in α corrections to the mass gaps, and in doing so find the Néel temperature curve, the order parameter φ_c, and full fluctuation corrections to the dispersions. To obtain corrections, we use an effective potential denoted by $\mathcal{V}$, which is the part of the Lagrangian (A1) independent of derivatives. Then, using a Wick decoupling of the interaction term $\frac{1}{4}\alpha_0\vec{\varphi}^4$, in the single loop approximation we find

$$\frac{\partial^2\mathcal{V}}{\partial\varphi_x^2} = m_0^2 - B^2 + 3\alpha_0\langle\varphi_x^2\rangle + \alpha_0\langle\varphi_y^2\rangle + \alpha_0\langle\varphi_z^2\rangle,$$

$$\frac{\partial^2\mathcal{V}}{\partial\varphi_y^2} = m_0^2 - B^2 + \alpha_0\langle\varphi_x^2\rangle + 3\alpha_0\langle\varphi_y^2\rangle + \alpha_0\langle\varphi_z^2\rangle,$$

$$\frac{\partial^2\mathcal{V}}{\partial\varphi_z^2} = m_0^2 + \alpha_0\langle\varphi_x^2\rangle + \alpha_0\langle\varphi_y^2\rangle + 3\alpha_0\langle\varphi_z^2\rangle, \tag{A2}$$

where $\langle\varphi_x^2\rangle$ is the loop integral over the Green's function of field φ_x: G_{xx}. An explicit calculation shows $\langle\varphi_x^2\rangle = \langle\varphi_y^2\rangle$. The bare Greens functions follow immediately from (A1), they are

$$G_{xx}(\omega,\boldsymbol{k}) = G_{yy}(\omega,\boldsymbol{k}) = \frac{\omega^2-k^2}{[\omega^2-(\omega_{\boldsymbol{k}}^+)^2][\omega^2-(\omega_{\boldsymbol{k}}^-)^2]},$$

$$G_{zz}(\omega,\boldsymbol{k}) = \frac{1}{\left[\omega^2-(\omega_{\boldsymbol{k}}^0)^2\right]},$$

$$G_{xy}(\omega,\boldsymbol{k}) = G_{yx}^*(\omega,\boldsymbol{k}) = \frac{2i\omega B}{[\omega^2-(\omega_{\boldsymbol{k}}^+)^2][\omega^2-(\omega_{\boldsymbol{k}}^-)^2]}, \tag{A3}$$

with dispersions $\omega_{\boldsymbol{k}}^\sigma$ as defined in the main text (4).

APPENDIX B: RUNNING COUPLING CONSTANT

The four point vertex is calculated to second order in α, the infrared cutoff Λ is given by the mass, the magnetic field, or the temperature scale: $\max\{m_\Lambda, B, T\}$. We use a Callan-Symanzik equation to find the Beta function

$$\Gamma^{(4)} = \alpha - 11\alpha^2\int_\Lambda^{\Lambda_c}\frac{d^4k}{(2\pi)^4}\frac{1}{k^4},$$

$$0 = \left[\frac{d}{d\ln(\Lambda_c/\Lambda)} + \beta(\alpha)\frac{d}{d\alpha}\right]\Gamma^{(4)},$$

$$\alpha_\Lambda = \frac{\alpha_0}{1 + \frac{11\alpha_0}{8\pi^2}\ln(\Lambda_0/\Lambda)}, \tag{B1}$$

where Λ_c is some momentum cutoff such as the inverse lattice spacing, while Λ_0 is the "normalization" scale or point.

APPENDIX C: RUNNING MASS

Consider the corrections to the curvature (A2), under renormalization, we replace the bare coupling with the running running coupling $\alpha_0 \to \alpha_\Lambda$, and now explicitly substituting loop integrals (with $i = \{x,y\}$)

$$\frac{\partial^2\mathcal{V}}{\partial\varphi_i^2} = m_0^2 - B^2 + 5\alpha_\Lambda\int\frac{d^3k}{(2\pi)^3}\frac{1}{2\omega_{\boldsymbol{k}}^0}$$

$$+ \alpha_\Lambda\int\frac{d^3k}{(2\pi)^3}\frac{1}{\omega_{\boldsymbol{k}}^0}\{2n(\omega_{\boldsymbol{k}}^+) + 2n(\omega_{\boldsymbol{k}}^-) + n(\omega_{\boldsymbol{k}}^0)\},$$

$$\frac{\partial^2\mathcal{V}}{\partial\varphi_z^2} = m_0^2 + 5\alpha_\Lambda\int\frac{d^3k}{(2\pi)^3}\frac{1}{2\omega_{\boldsymbol{k}}^0}$$

$$+ \alpha_\Lambda\int\frac{d^3k}{(2\pi)^3}\frac{1}{\omega_{\boldsymbol{k}}^0}\{n(\omega_{\boldsymbol{k}}^+) + n(\omega_{\boldsymbol{k}}^-) + 3n(\omega_{\boldsymbol{k}}^0)\}. \tag{C1}$$

The coupling constant coefficient is the running coupling α_Λ, since the two point corrections are multiplicative with the four point vertices. The integral first terms in (C1) renormalize the bare mass term m_0^2, such that $m_0^2 + 5\alpha_\Lambda\int\frac{d^3k}{(2\pi)^3}\frac{1}{2\omega_{\boldsymbol{k}}} \to m_\Lambda^2$ has logarithmic dependence on the energy scale Λ. The second integral terms, or the "thermal perturbations," only contributes to the logarithmic running via its influence on the infrared cutoff. To make these statements more clear, consider zero temperature such that only the first term contributes. We write the two point function as (with forward substitution of running mass $m_0 \to m_\Lambda$)

$$\Gamma^{(2)} \equiv \frac{\partial^2\mathcal{V}}{\partial\varphi_z^2}\bigg|_{T=0} = m_\Lambda^2 + 5\alpha_\Lambda\int_\Lambda^{\Lambda_c}\frac{d^3k}{(2\pi)^3}\frac{1}{2\sqrt{k^2+m_\Lambda^2}}$$

$$= m_\Lambda^2 - \frac{5\alpha_\Lambda}{8\pi^2}m_\Lambda^2\ln\left(\frac{\Lambda_c}{\Lambda}\right) = \frac{\partial^2\mathcal{V}}{\partial\varphi_i^2}\bigg|_{T=0}$$

$$+ B^2. \tag{C2}$$

We note that the logarithmic correction is independent of magnetic field B, which is essential to ensure that B is not renormalized. We use the Callan-Symanzik equation to find the (mass) Beta function

$$0 = \left[\frac{d}{d\ln(\Lambda_c/\Lambda)} + \beta_m(\Lambda)\frac{d}{dm_\Lambda^2}\right]\Gamma^{(2)},$$

$$\beta_m(\Lambda) = \frac{5\alpha_\Lambda m_\Lambda^2}{8\pi^2},$$

$$\frac{dm_\Lambda^2}{d\ln(\Lambda_0/\Lambda)} = -\frac{5\alpha_\Lambda m_\Lambda^2}{8\pi^2},$$

$$m_{\Lambda,\sigma}^2 = m_0^2 \left(\frac{\alpha_\Lambda}{\alpha_0}\right)^{5/11}. \qquad \text{(C3)}$$

In this last line we explicitly give an index σ to denote the different polarizations. At zero temperature, the terms $m_{\Lambda,\sigma}$ are equivalent for all polarizations σ. Including nonzero temperatures does not change the form of the running coupling nor mass Eqs. (B1) and (C3), but it does: (i) influence the infrared cutoff from $\Lambda = \text{Max}\{m_\Lambda, B, T\}$; and (ii) lifts the degeneracy of the mass terms, which now explicitly becomes

$$m_{\Lambda,\pm}^2 = m_0^2 \left[\frac{\alpha_\Lambda}{\alpha_0}\right]^{5/11}$$
$$+ \alpha_\Lambda \sum_k \frac{1}{\omega_k^0}\left\{2n(\omega_k^+) + 2n(\omega_k^-) + n(\omega_k^0)\right\}, \quad \text{(C4)}$$

$$m_{\Lambda,z}^2 = m_0^2 \left[\frac{\alpha_\Lambda}{\alpha_0}\right]^{5/11}$$
$$+ \alpha_\Lambda \sum_k \frac{1}{\omega_k^0}\left\{n(\omega_k^+) + n(\omega_k^-) + 3n(\omega_k^0)\right\}. \quad \text{(C5)}$$

[1] M. P. A. Fisher, P. B. Weichman, G. Grinstein, and D. S. Fisher, Phys. Rev. B **40**, 546 (1989).

[2] D. I. Uzunov, Phys. Lett. A **87**, 11 (1981).

[3] T. Giamarchi and A. M. Tsvelik, Phys. Rev. B **59**, 11398 (1999).

[4] T. Nikuni, M. Oshikawa, A. Oosawa, and H. Tanaka, Phys. Rev. Lett. **84**, 5868 (2000).

[5] N. Kawashima, J. Phys. Soc. Jpn. **74**, 145 (2005).

[6] W. Shiramura, K. Takatsu, H. Tanaka, K. Kamishima, M. Takahashi, H. Mitamura, and T. Goto, J. Phys. Soc. Jpn. **66**, 1900 (1997).

[7] T. Kato, K. Takatsu, H. Tanaka, W. Shiramura, M. Mori, K. Nakajima, and K. Kakurai, J. Phys. Soc. Jpn. **67**, 752 (1998); A. Oosawa, T. Takamasu, K. Tatani, H. Abe, N. Tsujii, O. Suzuki, H. Tanaka, G. Kido, and K. Kindo, Phys. Rev. B **66**, 104405 (2002).

[8] A. Oosawa, M. Ishii, and H. Tanaka, J. Phys. Condens. Matter **11**, 265 (1999); N. Cavadini, G. Heigold, W. Henggeler, A. Furrer, H.-U. Güdel, K. Krämer, and H. Mutka, Phys. Rev. B **63**, 172414 (2001).

[9] H. Tanaka, A. Oosawa, T. Kato, H. Uekusa, Y. Ohashi, K. Kakurai, and A. Hoser, J. Phys. Soc. Jpn. **70**, 939 (2001).

[10] S. Wessel, M. Olshanii, and S. Haas, Phys. Rev. Lett. **87**, 206407 (2001).

[11] O. Nohadani, S. Wessel, B. Normand, and S. Haas, Phys. Rev. B **69**, 220402(R) (2004)

[12] N. Kurita and H. Tanaka, Phys. Rev. B **94**, 104409 (2016).

[13] J. Sirker, A. Weiße, and O. P. Sushkov, J. Phys. Soc. Jpn. **74**, 129 (2005).

[14] For a review see H. Shi and A. Griffin, Phys. Rep. **304**, 1 (1998).

[15] S. Sachdev, *Quantum Phase Transitions* (Cambridge University Press, Cambridge, 2011).

[16] Y. Kulik and O. P. Sushkov, Phys. Rev. B **84**, 134418 (2011).

[17] Ch. Rüegg, N. Cavadini, A. Furrer, K. Krämer, H.-U. Güdel, P. Vorderwisch, and H. Mutka, Appl. Phys. A **74**, S840 (2002).

[18] Ch. Rüegg, N. Cavadini, A. Furrer, H.-U. Güdel, K. Krämer, H. Mutka, A. Wildes, K. Habicht, and P. Vorderwisch, Nature (London) **423**, 62 (2003).

[19] H. D. Scammell and O. P. Sushkov, Phys. Rev. B **92**, 220401(R) (2015).

[20] Due to a small anisotropy, the g factor slightly depends on the direction of magnetic field with respect to the crystal axes. We use BEC data with magnetic field directed as per experiment.

[21] J. Zinn-Justin. *Quantum Field Theory and Critical Phenomena* (Oxford University Press, Oxford, 2002).

[22] A. Oosawa, H. Aruga Katori, and H. Tanaka, Phys. Rev. B **63**, 134416 (2001).

[23] Y. Shindo and H. Tanaka, J. Phys. Soc. Jpn. **73**, 2642 (2004).

[24] Ch. Rüegg, B. Normand, M. Matsumoto, A. Furrer, D. F. McMorrow, K. W. Krämer, H. U. Güdel, S. N. Gvasaliya, H. Mutka, and M. Boehm, Phys. Rev. Lett. **100**, 205701 (2008).

[25] F. Yamada, T. Ono, H. Tanaka, G. Misguich, M. Oshikawa, and T. Sakakibara, J. Phys. Soc. Jpn. **77**, 013701 (2008).